CHEMISTRY
A European Journal

A Journal of
ChemPubSoc Europe

## Accepted Article

**Title:** HKUST-1 derived hollow C-Cu2-xS nanotube/g-C3N4 composites for visible-light CO2 photoreduction with H2O vapor

**Authors:** Cheng-Ying Hu, Jie Zhou, Chun-Yi Sun, Meng-meng Chen, Xin-Long Wang, and Zhong-Min Su



**To be cited as:** *Chem. Eur. J.* 10.1002/chem.201804925

**Link to VoR:** http://dx.doi.org/10.1002/chem.201804925

Supported by
ACES

WILEY-VCH

10.1002/chem.201804925

FULL PAPER

WILEY-VCH

# HKUST-1 derived hollow C-$Cu_{2-x}S$ nanotube/g-$C_3N_4$ composites for visible-light $CO_2$ photoreduction with $H_2O$ vapor

Cheng-Ying Hu[a], Jie Zhou[a], Chun-Yi Sun[a,*], Meng-meng Chen[a], Xin-Long Wang[a,b,*] and Zhong-Min Su[a,b]

**Abstract:** As the main component of syngas, reducing $CO_2$ to CO with high selectivity through photocatalysis could provide a sustainable way to alleviate energy shortage issues. Developing a photocatalytic system with low-cost, high-performance and environment-friendly is the ultimate goal towards $CO_2$ photoreduction. Herein, an efficient and economic three-component heterojunction photocatalyst is designed and fabricated for converting $CO_2$ to CO in absence of organic sacrifice agents, made of $Cu_{2-x}S$ nanotube coated carbon layer (C-$Cu_{2-x}S$) and g-$C_3N_4$. Using classical MOF material HKUST-1 as a precursor, hollow tubular-like metal sulfides (C-$Cu_{2-x}S$) with carbon coat were synthesized and further loaded on g-$C_3N_4$ forming a three-component heterojunction C-$Cu_{2-x}S$@g-$C_3N_4$. The carbon coat in C-$Cu_{2-x}S$@g-$C_3N_4$ acting as electron reservoir facilitates electron-hole pair separation. The optimized C-$Cu_{2-x}S$@g-$C_3N_4$ as a photocatalyst in $CO_2$ reduction performed a high reactivity of 1062.6 $\mu$mol·$g^{-1}$ and selectivity of 97%. Compared to bare g-$C_3N_4$ (158.4 $\mu$mol·$g^{-1}$) and C-$Cu_{2-x}S$, the reactivity is nearly 7 and 23-fold enhancement and this CO generation rate is higher than most of reported $Cu_2S$ or g-$C_3N_4$ composites under similar condition. The prominent activity may result from enhanced light adsorption and effective charge separation. This work might open up an alternative method to design and fabrication of high performance and low-cost photocatalyst for efficiently and durably converting $CO_2$ to CO with high selectivity.

## Introduction

Chemical reduction of carbon dioxide ($CO_2$) into valued-added chemicals can not only be a strategy to reduce the density of $CO_2$ in the atmosphere but provide a sustainable venue to generate renewable energy.[1] Photocatalysis and electrocatalysis are regarded as two effective methods to realize the conversion. For electrocatalysis, the actual application is mainly restricted by the high-cost energy input while for photocatalysis, the free and abundant sunlight could be used as the clean power source.[2] As one type of product in $CO_2$ reduction, carbon monoxide (CO) attracts great attention because it is a valuable raw material of syngas. Syngas is an important material for the production of liquid fuels and traditional technology usually depends on the reformation of fossil fuels.[3] Therefore, photocatalytic reduction of $CO_2$ to high-purity CO is considered to be a promising approach for global energy generation in a sustainable and clean way. At present, there are few reports on high-purity CO photo-generation which may largely due to the small difference in potential energy of various products during $CO_2$ reduction.[4] What's more, hydrogen ($H_2$) production is a common competitive reaction for CO generation.[5]

More recently, two-dimensional nanostructured semiconductors with high chemical stability, nontoxicity and low cost are explored as photocatalysts for $CO_2$ reduction.[6] Among them, the application of graphitic carbon nitride (g-$C_3N_4$) in $CO_2$ reduction undergoes an explosive development for its easily available, abundant, appropriate band edge and environment-friendly.[7] Despite these advantages, pure g-$C_3N_4$ exhibits low reductive efficiency in the photo-reduction of $CO_2$, mainly due to the limited visible-light adsorption and high recombination rate of photoinduced electrons-holes. Fabricating heterojunction material is a promising way to resolve these issues.[8] Up to now, plenty of g-$C_3N_4$-based composites, such as $TiO_2$/g-$C_3N_4$, TaON/g-$C_3N_4$, CdS/g-$C_3N_4$, $MoO_3$/g-$C_3N_4$, $Ag_3PO_4$/g-$C_3N_4$, $SnO_{2-x}$/g-$C_3N_4$ and BiOCl/g-$C_3N_4$, have been reported.[9] However, most current photocatalytic systems with g-$C_3N_4$-based composite as photocatalysts require additional organic sacrificial agents and/or organic solvent, which add an extra burden to both economy and environment.[10] Therefore, exploring new types of photocatalysts which can be active in water condition without any organic chemicals is urgent.

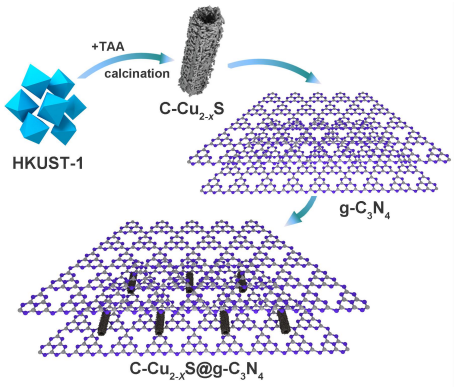


**Figure 1.** A schematic illustration of the fabrication of C-$Cu_{2-x}S$@g-$C_3N_4$ composites.

[a]C.-Y, Hu, J. Zhou, C.-Y. Sun, M.-M. Chen, Prof. X.-L. Wang, Prof. Z.-M. Su
National & Local United Engineering Laboratory for Power Batteries, Key Laboratory of Polyoxometalate Science of Ministry of Education
Department of Chemistry, Northeast Normal University
Changchun, Jilin, 130024 (P.R. China)
E-mail: suncy009@nenu.edu.cn; wangxl824@nenu.edu.cn
[b]Z.-M. Su
Changchun University of Science and Technology

Supporting information for this article is given via a link at the end of the document.

10.1002/chem.201804925





Herein, a three-component heterojunction photocatalyst, carbon coated copper(I) sulphide loading on g-$C_3N_4$ (C-$Cu_{2-x}S$@g-$C_3N_4$), was designed for $CO_2$ photoreduction owing to the excellent light absorbing property of $Cu_2S$ and the advantage of carbon layers on facilitating charge separation. To fabricate such structure, classical copper content metal-organic framework (MOF) material, HKUST-1, was selected as the precursor of C-$Cu_{2-x}S$. Through convenient sulfidation and calcination, C coated $Cu_{2-x}S$ (C-$Cu_{2-x}S$) with hollow architecture were obtained. Via mixing C-$Cu_{2-x}S$ with g-$C_3N_4$ under heating, the three-component C-$Cu_{2-x}S$@g-$C_3N_4$ photocatalyst was fabricated and the hollow structure of C-$Cu_{2-x}S$ was preserved (Figure 1). Under visible-light irradiation and water vapor condition, $CO_2$ could be efficiently reduced into CO by C-$Cu_{2-x}S$@g-$C_3N_4$-2 with a yield up to 1062.6 $\mu$mol·$g^{-1}$ which outperform most of reported $Cu_2S$ or g-$C_3N_4$ composites. As the common competing reaction in $CO_2$ photoreduction, $H_2$ evolution was effectively suppressed in our system and the selectivity toward CO was higher than 97 % which is quite rare in g-$C_3N_4$ based $CO_2$ photoreduction. Mechanism studies reveal enhanced light adsorption and facilitated separation of electron-hole pairs may ascribe to the high reductive activity.

## Results and Discussion

For fabrication of the targeted three-component photocatalyst material, classical copper content MOF material, HKUST-1, was selected as the precursor for C-$Cu_{2-x}S$ based on the ordered arrangement of copper nodes and carbon-rich organic ligand in HKUST-1. Through mixing HKUST-1 and TAA under stir and further calcination, C coated $Cu_{2-x}S$ was obtained. Comparing with traditional methods for synthesis of carbon-doped $Cu_{2-x}S$ which usually need complicated steps, extra template and harsh condition, such as high concentration of the alkaline solution, this method is convenient and nano-sized carbon layer could be directly introduced into $Cu_{2-x}S$. The three-component composite material was obtained under hydrothermal condition containing C-$Cu_{2-x}S$ and g-$C_3N_4$. Employing different weight ratios of C-$Cu_{2-x}S$ and g-$C_3N_4$, the three-component composites of C-$Cu_{2-x}S$@g-$C_3N_4$ with different content of C-$Cu_{2-x}S$ were fabricated. As determined by inductively coupled plasma mass spectrometry (ICP-MS), the corresponding C-$Cu_{2-x}S$ content in the resultant C-$Cu_{2-x}S$@g-$C_3N_4$ composites was 0.32 wt%, 0.71 wt% and 2.89 wt% based on Cu content and labeled as C-$Cu_{2-x}S$@g-$C_3N_4$-1, C-$Cu_{2-x}S$@g-$C_3N_4$-2 and C-$Cu_{2-x}S$@g-$C_3N_4$-3 (Table S1).

The powder XRD pattern of synthesized g-$C_3N_4$, C-$Cu_{2-x}S$ and C-$Cu_{2-x}S$@g-$C_3N_4$ were shown in Figure 2a. The sharp peaks could be seen from the figure, which implies the good crystallinity of these materials. The diffraction peaks of C-$Cu_{2-x}S$ between 20 and 80° (23.64, 26.23, 27.36, 30.82, 31.52, 32.59, 39.07, 39.78, 45.40, 46.08, 48.55, 51.54, 53.64, 66.62) matched well with the characteristic peaks in tetragonal $Cu_{1.81}S$ (JCPDS card No. 41-0959) and the peaks between 10 and 40° (27.96, 28.86, 33.62, 35.44, 36.34, 37.62) were corresponded to djurleite $Cu_{31}S_{16}$ (JCPDS card No. 42-0564). For the composite material, the peaks at 13.2 and 27.4 were ascribed to g-$C_3N_4$ and the peaks at 26.2 37.5, 46.1, 48.5 and 53.9 corresponded to $Cu_{1.81}S$ and $Cu_{31}S_{16}$.[11]

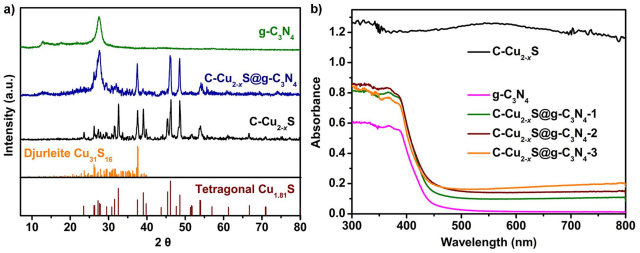


**Figure 2.** (a) X-ray diffraction (XRD) patterns of g-$C_3N_4$, C-$Cu_{2-x}S$ and C-$Cu_{2-x}S$@g-$C_3N_4$. (b) UV-Vis spetra of the C-$Cu_{2-x}S$, g-$C_3N_4$ and C-$Cu_{2-x}S$@g-$C_3N_4$-1, 2, 3.

The morphology of C-$Cu_{2-x}S$ and the composite material were investigated by scanning electron microscopy (SEM) and transmission electron microscopy (TEM). As shown in Figure 3a, the C-$Cu_{2-x}S$ presented a tubular structure assembled by nanorods and nanoparticles. The nano-tubular structure of C-$Cu_{2-x}S$ and nanosheet morphology of g-$C_3N_4$ (Figure S2) was preserved in the three-component composite (Figure 3b). The hollow structure may enlarge light-adsorption and surface area and provide multiple reactive sites. TEM further provided information about the tubular structure of C-$Cu_{2-x}S$ in g-$C_3N_4$ (Figure 3c and 3d). High-resolution TEM (Figure 3c, embedded imagine) reveal the microstructure of C-$Cu_{2-x}S$ from which carbon coat and two clear lattice fringes of C-$Cu_{2-x}S$ could be observed clearly. The interplanar spaces were nearly 0.378 and 0.239 nm, which were consistent with the typical interplanar space of $Cu_{1.81}S$ and $Cu_{31}S_{16}$, respectively. The elemental mappings (Figure 3e-g) of C-$Cu_{2-x}S$ clearly proved the existence of Cu, S and C in the C-$Cu_{2-x}S$ and we could see an average distribution of carbon in the composite from Figure 3g.

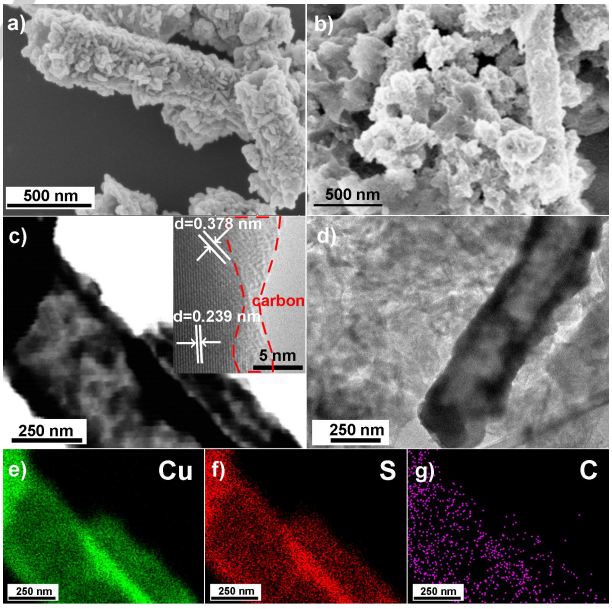


**Figure 3.** Scanning electron microscopy (SEM) images of (a) C-$Cu_{2-x}S$ and (b) the composite C-$Cu_{2-x}S$@g-$C_3N_4$-2. (c) transmission electron microscopy (TEM) pattern of the C-$Cu_{2-x}S$ nanotube. (d) TEM pattern of C-$Cu_{2-x}S$@g-$C_3N_4$-2 (e-g) energy dispersive X-ray (EDX) mappings of the C-$Cu_{2-x}S$ nanotube.

X-ray photoelectron spectroscopy (XPS) is further employed to determine the atomic valence states and bonding environment in C-$Cu_{2-x}S$ and C-$Cu_{2-x}S$@g-$C_3N_4$. The XPS survey spectrum of C-$Cu_{2-x}S$ is shown in Figure S3. The Cu 2p spectra show two characteristic peaks with a splitting width (19.9 eV) in Figure S3 corresponding to Cu $2p_{3/2}$ and Cu $2p_{1/2}$, which illuminates the oxidation state of Cu is $Cu^+$. The characteristic peaks at 161.2 and 162.4 eV ascribe to S $2p_{1/2}$ and S $2p_{3/2}$ of the S 2p suggesting the formation of metal sulfide. The peak centering at 163.8 eV is indicative of Cu-defect of non-stoichiometric copper sulfide (Figure S3).[12] Figure 4 presents the bonding environment in C-$Cu_{2-x}S$@g-$C_3N_4$. Figure 4a and 4b show typical peaks corresponding to copper sulphide. In addition, there are two satellite peaks at 942.2 eV and 962.1 eV indicating the presence of a small amount of $Cu^{2+}$. In Figure 4c, the C 1s XPS spectrum shows three peaks with the binding energies of 284.6, 285.3 and 288.0 eV, respectively. The peak centered at 284.6 eV is assigned to the C-C coordination originating from the adventitious carbon of the XPS instrument itself. For the peak locating at 285.3 eV with low intensity might be attributed to C-$NH_2$ and the peak emerging at 288.0 eV could be assigned to the N-C=N bonds of g-$C_3N_4$.[13] The N 1s could be fitted into four peaks (Figure 4d). Among them, three peaks located at 398.5, 399.9 and 401.1 eV could be attribute to C=N-C, tertiary nitrogen N-$(C)_3$ and amino functional groups with a hydrogen atom (C–N–H) of g-$C_3N_4$ respectively. The peak at 404.0 eV could be regarded as π-excitations.[14]

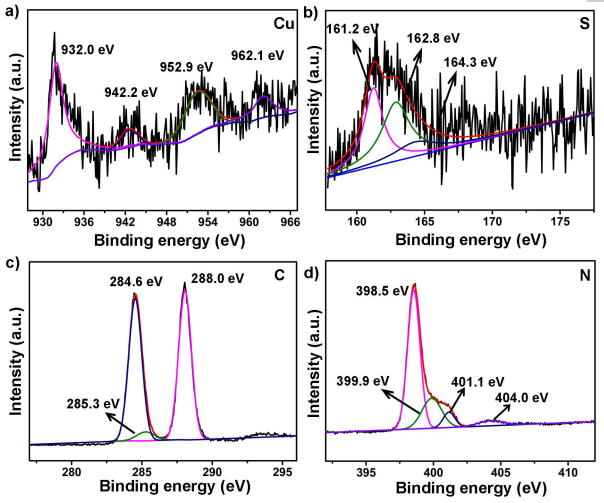


**Figure 4.** X-ray photoelectron spectroscopy (XPS) survey spectrum of (a) Cu, (b) S, (c) C and (d) N of C-$Cu_{2-x}S$@g-$C_3N_4$.

The surface area and pore size distributions of pure g-$C_3N_4$ and the resultant C-$Cu_{2-x}S$@g-$C_3N_4$-2 are characterized by nitrogen adsorption-desorption isotherms (Figure S4). Both of them exhibit type-IV sorption isotherms with hysteresis loop, which indicates the existence of mesopores in these samples.[15] The BET surface area and pore volume of pure g-$C_3N_4$ are about 61.2 $m^2 \cdot g^{-1}$ and 0.237 $cc \cdot g^{-1}$. Comparing with g-$C_3N_4$, the BET and pore volume of C-$Cu_{2-x}S$@g-$C_3N_4$ enhance around 50 %, up to 95.1 $m^2 \cdot g^{-1}$ and 0.313 $cc \cdot g^{-1}$. This increase might come from the hollow C-$Cu_{2-x}S$. These results illuminate that the loading of C-$Cu_{2-x}S$ could evidently enhance the surface area of composite material which will bring about more reactive sites for reduction reaction.

UV-VIS diffuse reflectance spectrum provides insightful information into the interactions between photocatalyst and photons which is a prerequisite process for $CO_2$ reduction (Figure 2b). The spectra of g-$C_3N_4$, C-$Cu_{2-x}S$ and the three-component composite were measured. Pure C-$Cu_{2-x}S$ has strong absorption to the whole visible light. Benefiting from the excellent visible-light adsorption ability of C-$Cu_{2-x}S$, all of the C-$Cu_{2-x}S$@g-$C_3N_4$ hybrids have an obvious absorption from 300 to 800 nm and the adsorption intensity within 300 to 450 nm is much stronger than bare g-$C_3N_4$. What's more, with the increase of loading content of C-$Cu_{2-x}S$, absorption intensity between 460 to 800 nm enhances. Therefore, it could be expected that the C-$Cu_{2-x}S$@g-$C_3N_4$ possesses outstanding visible-light catalytic activity.

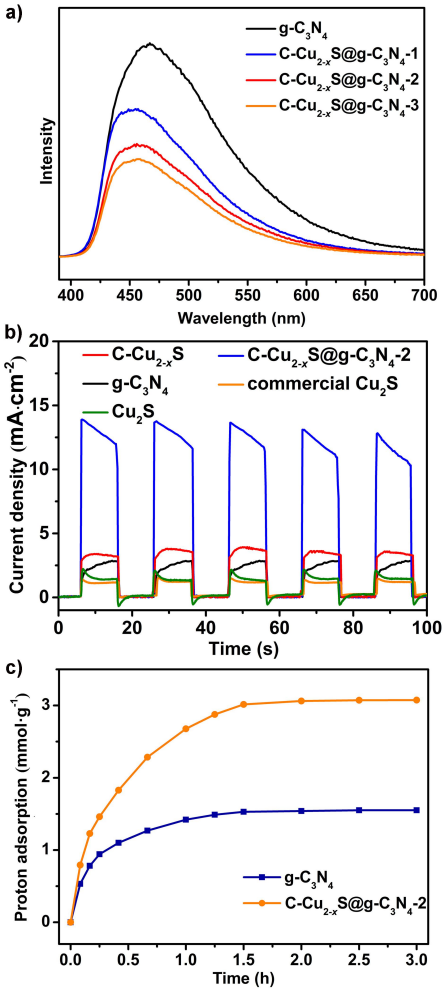


**Figure 5.** (a) Room temperature photoluminescence spectra of pure g-$C_3N_4$ and C-$Cu_{2-x}S$@g-$C_3N_4$-1, 2, 3 under the excitation wavelength of 390 nm. (b) Transient photocurrent response of C-$Cu_{2-x}S$, g-$C_3N_4$, $Cu_2S$, C-$Cu_{2-x}S$@g-$C_3N_4$-2 and commercial $Cu_2S$. (c) $H^+$ adsorption of g-$C_3N_4$ and C-$Cu_{2-x}S$@g-$C_3N_4$-2.

The photoluminescence (PL) spectra of g-$C_3N_4$ and C-$Cu_{2-x}S$@g-$C_3N_4$ composite is measured to evaluate the separation rate of photo-induced electrons and holes pairs after loading of

C-$Cu_{2-x}S$. Figure 5a shows the PL spectra of pure g-$C_3N_4$ and C-$Cu_{2-x}S$@g-$C_3N_4$ composites under an excitation wavelength of 390 nm at room temperature. Pure g-$C_3N_4$ shows a strong broad emission band peaking at 460 nm. As for C-$Cu_{2-x}S$@g-$C_3N_4$, the emission structure was preserved but with a low emission intensity and the intensity was decreased with the enhanced content of C-$Cu_{2-x}S$. This result implied that composite materials may possess a lower recombination rate of photo-excited electrons-holes and revealed the introduction of C-$Cu_{2-x}S$ could accelerate the charge transfer process.[16]

The positive effect of introducing C-$Cu_{2-x}S$ into g-$C_3N_4$ on charge separation was further revealed through transient photocurrent responses of C-$Cu_{2-x}S$@g-$C_3N_4$, bare g-$C_3N_4$ and C-$Cu_{2-x}S$. As presented in Figure 5b, the curve of transient photocurrent responses of bare C-$Cu_{2-x}S$ shows around 3.3 $\mu A \cdot cm^{-2}$ current density after irradiation, which is comparable to bare g-$C_3N_4$ but much higher than commercial $Cu_2S$ and synthesized tubular $Cu_2S$. This enhancement of C-$Cu_{2-x}S$ may result from the carbon coat which acting as electron pool facilitates the electrons separation generated by $Cu_{2-x}S$. For C-$Cu_{2-x}S$@g-$C_3N_4$, within five cycles, the current density is four-fold higher than the pure g-$C_3N_4$ and C-$Cu_{2-x}S$, up to 13.2 $\mu A \cdot cm^{-2}$ indicating the three-component materials achieve more efficient separation of electron-hole pairs.[17]

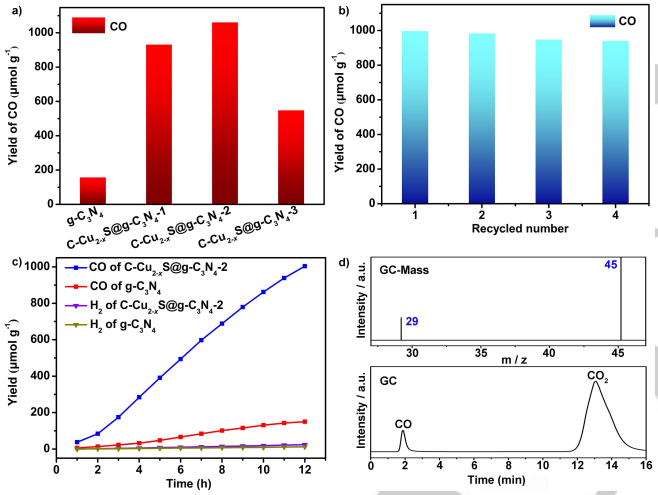


**Figure 6.** (a) Photocatalytic yield of pure g-$C_3N_4$ and C-$Cu_{2-x}S$@g-$C_3N_4$-1,2,3 (b) cycling runs for the photocatalytic CO evolution under visible light irradiation (c) time course of CO evolution (d) GC-Mass result of the isotopic experiment under $^{13}CO_2$ atmosphere and the corresponding GC spectrum of GC-Mass.

Photocatalytic reduction activities of $CO_2$ were carried out in a gas-sealed reactor under water vapor and visible-light irradiation for 12 h. During the photo-reduction process, trace amount $H_2$ was detected and CO was generated as the main gas product. Under visible-light irradiation, CO evolution rate of bare g-$C_3N_4$ and C-$Cu_{2-x}S$@g-$C_3N_4$ is shown in Figure 6. It is quite clear that the loading content of C-$Cu_{2-x}S$ has a significant impact on the photocatalytic activity of CO generation: (i) when C-$Cu_{2-x}S$ is loaded on g-$C_3N_4$ with a content of 0.32 wt %, the photocatalytic yield of CO was sharply increased from 158.4 $\mu mol \cdot g^{-1}$ (bare g-$C_3N_4$) to 932.8 $\mu mol \cdot g^{-1}$; (ii) with the content of C-$Cu_{2-x}S$ up to 0.71 wt %, the CO production rose to 1062.6 $\mu mol \cdot g^{-1}$ which was nearly seven folds higher than bare g-$C_3N_4$; (iii) with a further enhancement of C-$Cu_{2-x}S$ to 2.89 wt %, the generation underwent an obvious decrease reaching 549 $\mu mol \cdot g^{-1}$ which may root in the aggregation of C-$Cu_{2-x}S$ (Figure S1). These results deduce loading content of C-$Cu_{2-x}S$ has an influence on the CO generation and the optimal loading amount of C-$Cu_{2-x}S$ was 0.71 wt % with a generation rate of CO 88.5 $\mu mol \cdot h^{-1} \cdot g^{-1}$ and a selectivity of 97 %.

The isotopic experiment is carried out to illuminate the source of generated CO by using $^{13}CO_2$ as gas atmosphere under the similar photocatalytic conditions. As exhibited in Figure 6d, peaks at 1.88 min and 13.08 min with m/z 29 and 45 assign to $^{13}CO$ and $^{13}CO_2$, respectively. No signal at m/z = 28 appeared. This information provides direct evidence that the produced CO was generated from photoreduction of $CO_2$.

To further confirm the importance of C-$Cu_{2-x}S$@g-$C_3N_4$ in $CO_2$ photoreduction, control experiments are carried out under a similar condition (Table 1). The generation amount of CO with C-$Cu_{2-x}S$ (enter 3) as a photocatalyst is 45.56 $\mu mol \cdot g^{-1}$ while employing commercial $Cu_2S$ (enter 2) and synthesized tubular $Cu_2S$ (enter 4) as a photocatalyst, the amount decreases to 20.15 and 24.63 $\mu mol \cdot g^{-1}$, respectively, only half of the yield of C-$Cu_{2-x}S$. This result suggests that the carbon coat may play a positive role in enhancing the photocatalytic reactivity. When combining the commercial $Cu_2S$ with g-$C_3N_4$ named $Cu_2S$@g-$C_3N_4$ (enter 5), the production of CO is 436.83 $\mu mol \cdot g^{-1}$ which is 2-fold lower than C-$Cu_{2-x}S$@g-$C_3N_4$. With $Cu_2S$@g-$C_3N_4$ composite as catalyst made of tubular $Cu_2S$ and g-$C_3N_4$ (enter 6), the yield is also quite lower than C-$Cu_{2-x}S$@g-$C_3N_4$. The preponderance of C-$Cu_{2-x}S$@g-$C_3N_4$ on $CO_2$ photoreduction might come from the carbon coat. When directly mixing C-$Cu_{2-x}S$ and g-$C_3N_4$ (enter 7), the yield of CO is five folds lower than C-$Cu_{2-x}S$@g-$C_3N_4$. The significant decrease implies the loose contact is insufficient for the reduction of $CO_2$. In the same catalytic system without water, the yield of CO was only 47.81 $\mu mol \cdot g^{-1}$ (enter 8). When there was no catalyst (enter 9), no light (enter 10) or using argon instead of $CO_2$ (enter 11) in the catalytic system, there was almost no output. Besides these, the reactivity of C-$Cu_{2-x}S$@g-$C_3N_4$ in $CO_2$ photoreduction outperforms than most of the reported g-$C_3N_4$ or copper sulfide based composites under similar condition (Table S2).

Cycle performance and stability of a photocatalyst are vital to practical application. To examine the durability of our catalyst, four-run cycling photocatalytic experiment of C-$Cu_{2-x}S$@g-$C_3N_4$ (0.71 wt %) is carried out. It could be concluded from Figure 6b that there is no significant decline in CO production in these cycles. After this experiment, the XRD pattern of the sample was collected (Figure S5). Comparing to the XRD pattern of the original sample, the characteristic peaks' intensity of C-$Cu_{2-x}S$@g-$C_3N_4$ became weaker after cycling. This might be due to the reduced crystallinity after photocatalysis. The $CO_2$ reduction activity of C-$Cu_{2-x}S$@g-$C_3N_4$ (0.71 wt %) is further studied via detecting the yield of CO within every hour. As a control, the activity of bare g-$C_3N_4$ was investigated, as well. For both bare g-$C_3N_4$ and C-$Cu_{2-x}S$@g-$C_3N_4$ (Figure 6c), the first hour doesn't exhibit significant output. This illustrates the photocatalytic system may need an activation process for light excitation and achieve the adsorption equilibrium of $H_2O$ and $CO_2$ molecules on the surface of the catalyst. After that, the yield of CO using C-$Cu_{2-x}S$@g-$C_3N_4$ as catalyst almost increases at a constant speed in linear. The total production of CO and $H_2$ up to 1003.5

$\mu$mol·g$^{-1}$ and 24.34 $\mu$mol·g$^{-1}$, the selectivity of CO is more than 97 %. For bare g-$C_3N_4$, obvious enhancement emerged after 3 hours' reaction which indicates that C-$Cu_{2-x}S$ may provide some active reaction sites in $CO_2$ reduction. The total generation amount of CO and $H_2$ with g-$C_3N_4$ as a catalyst is 150.4 $\mu$mol·g$^{-1}$ and 12.92 $\mu$mol·g$^{-1}$ corresponding to a selectivity of 92.09 % toward CO.

**Table 1** Variation of reference experiments conditions[a]

| Entry | CO ($\mu$mol·g$^{-1}$) | $H_2$ ($\mu$mol·g$^{-1}$) | Sel. (%)[b] |
|---|---|---|---|
| 1[c] | 1062.60 | 26.42 | 97.57 |
| 2[d] | 20.15 | 5.63 | 78.16 |
| 3[e] | 45.56 | 7.47 | 85.91 |
| 4[f] | 24.63 | 6.27 | 79.71 |
| 5[g] | 436.83 | 43.51 | 90.94 |
| 6[h] | 524.47 | 68.32 | 88.47 |
| 7[i] | 239.04 | 38.15 | 86.24 |
| 8[j] | 47.81 | < 0.0001 | – |
| 9[k] | < 0.0001 | < 0.0001 | – |
| 10[l] | < 0.0001 | < 0.0001 | – |
| 11[m] | < 0.0001 | < 0.0001 | – |

[a] Reaction conditions: $H_2O$ (0.10 mL), $CO_2$ (1 bar), photocatalyst (1 mg), 25 °C, 12 h, and $\lambda \geq 420$nm. [b] Selectivity = $n_{CO}/n_{(CO+H2)} \times 100$. [c] Using C-$Cu_{2-x}S$@g-$C_3N_4$-2 as catalyst. [d] Employing commercial $Cu_2S$ as catalyst. [e] Applying C-$Cu_{2-x}S$ (made from HKUST-1) as catalyst. [f] Applying $Cu_2S$ (tubular) as catalyst which synthesized according to the reported literature.[18] [g] Employing $Cu_2S$@g-$C_3N_4$ as photocatalyst, prepared by mixing g-$C_3N_4$ and commercial $Cu_2S$ in Teflon reactor heating in an oven at 150 °C for 12 h (Details were shown in ESI). [h] Using $Cu_2S$@g-$C_3N_4$ composite as catalyst made of tubular $Cu_2S$ and g-$C_3N_4$ through a similar procedure in [c] (Details were shown in ESI). [i] Using directly mixed C-$Cu_{2-x}S$ and g-$C_3N_4$ to replace C-$Cu_{2-x}S$@g-$C_3N_4$. [j] Without $H_2O$ vapour. [k] Without C-$Cu_{2-x}S$@g-$C_3N_4$. [l] In the dark. [m] Using Ar to replace $CO_2$.

The above experiments establish a high activity and selectivity of C-$Cu_{2-x}S$@g-$C_3N_4$ and pace C-$Cu_{2-x}S$@g-$C_3N_4$ as highly efficient and low-cost candidate catalyst for $CO_2$ photoreduction. To understand the rooted reason, the photocatalytic mechanism was investigated. The performance of a photocatalytic system in $CO_2$ reduction is dictated by the balance of thermodynamics and kinetics. It should be noticed that compared with one electron reductive process (converting $CO_2$ into $CO_2^{\bullet-}$), proton-coupled electron transfer processes is thermodynamically more favorable.[19] However, the proton participated route has a significant kinetic dependence on proton and electron density on the surface of catalysts. When performing the experiment of $H^+$ protons adsorption (Figure 5c), the initial $H^+$ protons capture speed of C-$Cu_{2-x}S$@g-$C_3N_4$ up to 158.4 $\mu$mol·g$^{-1}$ min$^{-1}$ is observed which is 2 orders of magnitude higher than the generation speed of CO (1.475 $\mu$mol·g$^{-1}$·min$^{-1}$). The affluent protons accumulated on the surfaces of the catalyst provide a guarantee for the successful reduction of $CO_2$ through the proton-coupled pathway.

Considering the reactivity of the other half-reaction, the oxidative process, also has considerable influence on the efficiency of the $CO_2$ reduction under $H_2O$ vapor condition. The oxidation process in the three-component catalytic system is studied. $O_2$ (~500 $\mu$mol·g$^{-1}$) and trace amount $H_2O_2$ was detected as the product which should originate from the $H_2O$ oxidative process. Therefore, in the $CO_2$ photoreduction system, $H_2O$ is the sacrifice agent to provide electrons.[20]

As for water oxidation, the challenge mainly roots in the $O_2$ release because it usually involves a four-proton coupled four-electron transfer process.[21] Although the four-electron process is thermodynamically more favorable than the two-electron way, the two electrons participated process is kinetically favored. The stepwise two electrons/two-step pathway is proposed as an optimum approach between thermodynamic and kinetic constraints for water oxidation. A significant issue toward the stepwise two electrons/two-step pathway is to incorporate co-catalyst to decompose $H_2O_2$ to $O_2$ and $H_2O$.[22] In the three-component catalytic system, g-$C_3N_4$ incorporated with carbon coat might fulfill the two electrons/two-step oxidation pathway. The oxidation product of $O_2$ and $H_2O_2$ was detected in the catalytic system of using C-$Cu_{2-x}S$@g-$C_3N_4$ as photocatalyst and RRDE experiments (Figure S6 and Figure S7) confirm that the oxidation reaction undergoes two electron process.

In photocatalysis, three steps are universally accepted, including light harvest, charge separation and transportation to surface sites, and triggering redox reactions.[23] In $CO_2$ reduction with C-$Cu_{2-x}S$@$C_3N_4$ as photocatalyst, C-$Cu_{2-x}S$ contributes most of the adsorbed photons while g-$C_3N_4$ could absorb the light before 450 nm. The carbon coat serving as electron reservoir takes an important role in accumulating the photo-induced electrons therefore efficiently suppressing the recombination of the generated electron–hole (e–h$^+$) pairs. The generated electrons transfer to the carbon coat and trigger the reductive reaction under the assistant of $H^+$ proton from water to produce CO while the left holes on g-$C_3N_4$ with the assistant of carbon layers perform the water oxidative reaction and generate $O_2$ via a two-electron/two-step pathway.[20a]

## Conclusions

In conclusion, we design and fabricate an economic three-component composite photocatalyst, made of carbon coated $Cu_{2-x}S$ and g-$C_3N_4$ for efficiently $CO_2$ reduction with water under visible-light irradiation. With HKUST-1 as a precursor, hollow tubular-like $Cu_{2-x}S$ with carbon coat is fabricated successfully and further loaded C-$Cu_{2-x}S$ on g-$C_3N_4$ with different amount forming a serial of three-component heterojunction C-$Cu_{2-x}S$@g-$C_3N_4$. Unlike bare g-$C_3N_4$ that only absorbs the light with $\lambda$ less than 450 nm, the resultant composites possess a good light adsorption ability ranging from 300 to 800 nm. As evidenced by photoluminescent property and transient photocurrent responses, C-$Cu_{2-x}S$@-$C_3N_4$ has more efficient charges separation than bare g-$C_3N_4$. When comparing the current density of C-$Cu_{2-x}S$ with commercial $Cu_2S$ and synthesized tubular $Cu_2S$, the important role of the carbon coat in facilitating the photo-induced electrons and holes separation is revealed. Under visible-light irradiation and water vapor condition, the optimized C-$Cu_{2-x}S$@g-$C_3N_4$-2 (0.71 wt % of C-$Cu_{2-x}S$) performed a high reactivity of 1062.6 $\mu$mol·g$^{-1}$ and selectivity of 97%. Compared to bare g-$C_3N_4$ (158.4 $\mu$mol·g$^{-1}$), the reactivity is a nearly 7-fold enhancement and outperforms most of reported $Cu_2S$ or g-$C_3N_4$ composites in $CO_2$ reduction under similar condition. The

prominent activity may result from enhanced light adsorption and effective charge separation. This work might open up an alternative method to design and fabrication of high performance, low-cost and environment-friendly photocatalyst for efficiently and durably converting $CO_2$ to CO with high selectivity.

## Experimental Section

### Synthesis of C-$Cu_{2-x}S$

HKUST-1 was firstly prepared following a reported literature.[24] Then HKUST-1 (0.40 g) was dispersed in anhydrous ethanol (40 ml) and stirred for 0.5 h. Thioacetamide (TAA, 0.46 g) was dissolved in anhydrous ethanol (20 ml) and mixed with the former solution. Then keep the mixture under stirring at 310 r·min$^{-1}$ for 8 h at 30 °C. After that, the mixture was filtered, washed three times with ethanol and dried at 100 °C for 6 h. The dark brown powder was obtained. Then the synthesized powder was calcined at 700 °C for 2 h with a nitrogen atmosphere. When annealed to room temperature, the black powder was received.

### Synthesis of g-$C_3N_4$ and C-$Cu_{2-x}S$@g-$C_3N_4$

Pure g-$C_3N_4$ was synthesized through thermal polymerization of urea under air atmosphere following the reported procedure.[25] Urea powder (10 g) was put into a crucible with a cover and then heated to 550 °C at a rate of 5 °C·min$^{-1}$, keeping this temperature for 2.5 h. G-$C_3N_4$ was received after cooling down to 25 °C. A desired amount of C-$Cu_{2-x}S$ (2.5, 5 and 25 mg) was added into g-$C_3N_4$ (500 mg) suspension under ultrasonic for 30 min. The mixture was then transferred to a Teflon reactor (100 mL) and heated at 150 °C for 12 h. After cooling to room temperature, the mixture was filtrated and the obtained solid was evaporated at a controlled temperature of 60 °C in an oven for 12 h.

## Acknowledgements

This work was financially supported by the NSFC of China (No. 21601032, 21771035, 21671034, and 21471027), Changbai Mountain Scholars of Jilin Province, the China Postdoctoral Science Foundation (2017M611295).

**Keywords:** Metal–organic frameworks • semiconductors • photocatalysis • reduction

[1] a) S. Guo, S. Zhao, X. Wu, H. Li, Y. Zhou, C. Zhu, N. Yang, X. Jiang, J. Gao, L. Bai, Y. Liu, Y. Lifshitz, S. T. Lee and Z. Kang, *Nat Commun* **2017**, *8*, 1828; b) H. Shi, G. Chen, C. Zhang and Z. Zou, *ACS Catalysis* **2014**, *4*, 3637-3643.

[2] a) J. C. Wang, H. C. Yao, Z. Y. Fan, L. Zhang, J. S. Wang, S. Q. Zang and Z. J. Li, *ACS Appl Mater Interfaces* **2016**, *8*, 3765-3775; b) J. Wu, Y. Huang, W. Ye and Y. Li, *Adv Sci* **2017**, *4*, 1700194; c) X. Zhao, J. Feng, J. Liu, J. Lu, W. Shi, G. Yang, G. Wang, P. Feng and P. Cheng, *Adv Sci (Weinh)* **2018**, *5*, 1700590.

[3] a) J. Hou, H. Cheng, O. Takeda and H. Zhu, *Energy & Environmental Science* **2015**, *8*, 1348-1357; b) Y.-P. Yuan, S.-W. Cao, Y.-S. Liao, L.-S. Yin and C. Xue, *Applied Catalysis B: Environmental* **2013**, *140-141*, 164-168; c) X. Zhao, J. Feng, J. Liu, W. Shi, G. Yang, G. C. Wang and P. Cheng, *Angew Chem Int Ed Engl* **2018**, *57*, 9790-9794.

[4] a) M. Gattrell, N. Gupta and A. Co, *Journal of Electroanalytical Chemistry* **2006**, *594*, 1-19; b) K. P. Kuhl, E. R. Cave, D. N. Abram and T. F. Jaramillo, *Energy & Environmental Science* **2012**, *5*, 7050; c) X. Zhao, H. Yang, P. Jing, W. Shi, G. Yang and P. Cheng, *Small* **2017**, *13*.

[5] M. Chen, L. Han, J. Zhou, C. Sun, C. Hu, X. Wang and Z. Su, *Nanotechnology* **2018**, *29*, 284003.

[6] a) S.-W. Cao, X.-F. Liu, Y.-P. Yuan, Z.-Y. Zhang, Y.-S. Liao, J. Fang, S. C. J. Loo, T. C. Sum and C. Xue, *Applied Catalysis B: Environmental* **2014**, *147*, 940-946; b) Y. Wang, Y. Xu, Y. Wang, H. Qin, X. Li, Y. Zuo, S. Kang and L. Cui, *Catalysis Communications* **2016**, *74*, 75-79; c) J. Zhao, Q. Wang, C. Sun, T. Zheng, L. Yan, M. Li, K. Shao, X. Wang and Z. Su, *Journal of Materials Chemistry A* **2017**, *5*, 12498-12505; d) J. Zhou, W. Chen, C. Sun, L. Han, C. Qin, M. Chen, X. Wang, E. Wang and Z. Su, *ACS Appl Mater Interfaces* **2017**, *9*, 11689-11695.

[7] a) S. Bai, X. Wang, C. Hu, M. Xie, J. Jiang and Y. Xiong, *Chem Commun (Camb)* **2014**, *50*, 6094-6097; b) J. Lin, Z. Pan and X. Wang, *ACS Sustainable Chemistry & Engineering* **2013**, *2*, 353-358; c) G. Zhao, H. Pang, G. Liu, P. Li, H. Liu, H. Zhang, L. Shi and J. Ye, *Applied Catalysis B: Environmental* **2017**, *200*, 141-149.

[8] a) C.-J. Chang, H.-T. Weng and C.-C. Chang, *International Journal of Hydrogen Energy* **2017**, *42*, 23568-23577; b) F. Cheng, H. Yin and Q. Xiang, *Applied Surface Science* **2017**, *391*, 432-439; c) F. He, G. Chen, Y. Yu, S. Hao, Y. Zhou and Y. Zheng, *ACS Appl Mater Interfaces* **2014**, *6*, 7171-7179.

[9] a) Y. Bai, P.-Q. Wang, J.-Y. Liu and X.-J. Liu, *RSC Advances* **2014**, *4*, 19456; b) S. Obregón and G. Colón, *Applied Catalysis B: Environmental* **2014**, *144*, 775-782; c) S. Patnaik, G. Swain and K. M. Parida, *Nanoscale* **2018**, *10*, 5950-5964; d) S. C. Yan, S. B. Lv, Z. S. Li and Z. G. Zou, *Dalton Trans* **2010**, *39*, 1488-1491; e) Y. M. He, L. H. Zhang, B. T. Teng and M. H. Fan, *Environ. Sci. Technol* **2015**, *49*, 649-656; f) Y. M. He, L. H. Zhang, M. H. Fan, X. X. Wang, M. L. Walbridge, Q. Y. Nong, Y. Wu and L. H. Zhao, *Solar Energy Materials & Solar Cells* **2015**, *137*, 175-184; g) J. Zhang, Y. Wang, J. Jin, J. Zhang, Z. Lin, F. Huang and J. Yu, *ACS Appl Mater Interfaces* **2013**, *5*, 10317-10324.

[10] R. Kuriki, O. Ishitani and K. Maeda, *ACS Appl Mater Interfaces* **2016**, *8*, 6011-6018.

[11] S. Zhou, Y. Liu, J. Li, Y. Wang, G. Jiang, Z. Zhao, D. Wang, A. Duan, J. Liu and Y. Wei, *Applied Catalysis B: Environmental* **2014**, *158-159*, 20-29.

[12] a) R. Wu, D. P. Wang, V. Kumar, K. Zhou, A. W. Law, P. S. Lee, J. Lou and Z. Chen, *Chem Commun (Camb)* **2015**, *51*, 3109-3112; b) Y. Xie, A. Riedinger, M. Prato, A. Casu, A. Genovese, P. Guardia, S. Sottini, C. Sangregorio, K. Miszta, S. Ghosh, T. Pellegrino and L. Manna, *J Am Chem Soc* **2013**, *135*, 17630-17637.

[13] J. Li, B. Shen, Z. Hong, B. Lin, B. Gao and Y. Chen, *Chem Commun (Camb)* **2012**, *48*, 12017-12019.

[14] Q. Lin, L. Li, S. Liang, M. Liu, J. Bi and L. Wu, *Applied Catalysis B: Environmental* **2015**, *163*, 135-142.

[15] X. Chen, H. Li, Y. Wu, H. Wu, L. Wu, P. Tan, J. Pan and X. Xiong, *J Colloid Interface Sci* **2016**, *476*, 132-143.

[16] S. Wang, B. Y. Guan and X. W. D. Lou, *J Am Chem Soc* **2018**, *140*, 5037-5040.

[17] X. An, K. Li and J. Tang, *ChemSusChem* **2014**, *7*, 1086-1093.

[18] Z. Yao, X. Zhu, C. Wu, X. Zhang and Y. Xie, *Crystal Growth & Design* **2007**, *7*, 1256-1261.

[19] a) B. Lin, S. Golshanshirazi, G. Guiochon, *J. Phys. Chem* **1989**, *93*, 3363-3368; b) H. A. Schwarz, R. W.Dodson, *J. Phys. Chem* **1989**, *93,* 409-414.

[20] a) L. Yu, G. J. Li, X. S. Zhang, X. Ba, G. D. Shi, Y. Li, P. K. Wong, J. C. Yu and Y. Yu, *ACS Catalysis* **2016**, *6*, 6444-6454; b) P. Kar, S. Farsinezhad, X. J. Zhang and K. Shankar, *Nanoscale* **2014**, *6*, 14305-14318; c) L. L. Tan, W. J. Ong, S. P. Chai and A. R. Mohamed, *Chemical Engineering Journal* **2017**, *308*, 248-255; d) H. Wang, Z. Sun, Q. Li, Q. Tang and Z. Wu, *Journal of $CO_2$ Utilization* **2016**, *14*, 143-151.

[21] X. Chang, T. Wang and J. Gong, *Energy & Environmental Science* **2016**, *9*, 2177-2196.

[22] J. Liu, Y. Liu, J. Li, N. Liu, Y. Han, X. Zhang, H. Huang, Y. Lifshitz, S. T. Lee, J. Zhong and Z. Kang, *Science* **2015**, *347*, 970-974.

10.1002/chem.201804925





[23] T. Hisatomi, J. Kubota and K. Domen, *Chem Soc Rev* **2014**, *43*, 7520-7535.
[24] J. Gascon, S. Aguado and F. Kapteijn, *Microporous and Mesoporous Materials* **2008**, *113*, 132-138.
[25] S. Cao, J. Low, J. Yu and M. Jaroniec, *Adv Mater* **2015**, *27*, 2150-2176.

10.1002/chem.201804925



WILEY-VCH

## Entry for the Table of Contents

# FULL PAPER

Load tubular C-$Cu_{2-x}S$ onto g-$C_3N_4$ nanosheet to form a three-component catalyst and performing photocatalytic reduction of $CO_2$.

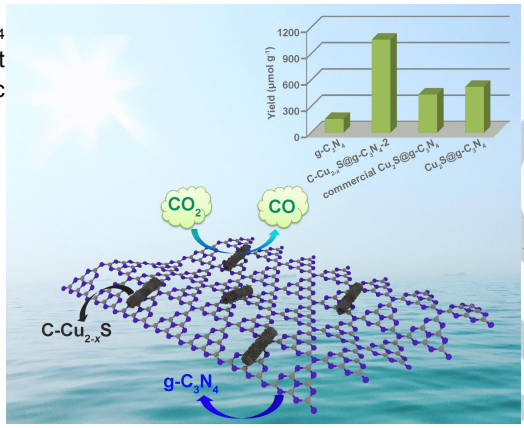


*Cheng-Ying Hu, Jie Zhou, Chun-Yi Sun*, Meng-Meng Chen, Xin-Long Wang* and Zhong-Min Su*

***Page No. – Page No.***

**HKUST-1 derived hollow C-$Cu_{2-x}S$ nanotube/g-$C_3N_4$ composites for visible-light $CO_2$ photoreduction with $H_2O$ vapor**